Nonreciprocal spin waves driven by left-hand microwaves

Zhizhi Zhang, Zhenyu Wang, Huanhuan Yang, Z.-X. Li, Yunshan Cao, and Peng Yan*
School of Electronic Science and Engineering and State Key Laboratory of Electronic Thin Films and Integrated Devices, University of Electronic Science and Technology of China, Chengdu 610054, China

(Received 29 January 2022; revised 22 October 2022; accepted 25 October 2022; published 14 November 2022)

It is conventional wisdom that a left-hand microwave cannot efficiently excite the spin wave (SW) in the ferromagnet due to the constraint of angular momentum conservation. In this work, we show that the left-hand microwave can drive nonreciprocal SWs in the presence of a strong ellipticity mismatch between the microwave and processing magnetization. A compensation frequency is predicted, at which the left-hand microwave cannot excite SWs. Away from it the SW amplitude sensitively depends on the microwave ellipticity, in sharp contrast to the case driven by right-hand microwaves. By tuning the driving frequency, we observe a switchable SW nonreciprocity in the ferromagnetic layer. A mode-dependent mutual demagnetizing factor is proposed to explain this finding. Our work advances the understanding of photon-magnon conversion and paves the way to designing diodelike nanoscale magnonic devices.

DOI: 10.1103/PhysRevB.106.174413

I. INTRODUCTION

Magnonics is an emerging field aiming for future low-loss wave-based information processing [1–7]. Among the splendid magnonic functionalities, chirality and nonreciprocity serve as building blocks [8–12] for the integrated magnonic circuits since the spin precession is innately chiral [13–15]. The nonreciprocity takes root in the magnetodipolar interaction via, for example, the well-known Damon-Eshbach (DE) geometry [16–19], bilayer magnets and inhomogeneous thin films [20–27], and magnetic heterostructures in the presence of magnetoelastic or magneto-optic coupling [28–31]. However, with the isotropic exchange interaction dominating in the microscale region [32–34], the dipolar effect, followed by the induced nonreciprocity, is vanishingly small [35]. The nonreciprocity can also emerge in the chiral edge states of elaborately devised topological magnetic materials or spin-texture arrays, which are robust to defects and disorders [36–41]. But it requires specific lattice designs and complicated couplings between atoms or elements, and the confined magnon (the quantum of the spin wave) channels at the edges reduce the usage of magnetic systems. Another origin of the nonreciprocity comes from the Dzyaloshinskii-Moriya interaction (DMI) [42]. However, the effect is negligibly weak in ferromagnetic insulators, like yttrium iron garnet (YIG, $Y_3Fe_5O_{12}$) [43]. Additional heavy metal structures can introduce a sizable DMI [44–46] but inevitably bring remarkably increased damping and Joule heating [47].

To realize efficient excitation of the nonreciprocal short-wavelength dipolar-exchange or even pure-exchange spin waves (SWs) in ferromagnetic insulators to miniaturize magnonic devices, several methods have been suggested [48–54]. Conventionally, the coherent SW excitation harnesses microwave antennas with the exciting field linearly polarized and uniform across the film thickness. Since the in-plane component of microwave fields dominantly contributes to the excitations, it is solely accounted for in the analysis [55–58]. By contrast, the dynamic fields generated by micromagnetic structures are not only highly localized at interfaces favoring short-wavelength SW excitation [59–61] but also polarized with complex chiralities. Yu *et al.* reported an analysis of the chiral pumping (excitation) of exchange magnons in YIG into (from) the proximate magnetic wires via directional dipolar interactions [62,63]. A selection rule is adopted that circular magnons and photons with the same (opposite) chiralities are allowed (forbidden) to interact [30]. One critical issue is how microwave fields with opposite chirality can excite the propagating SWs.

In this work, we theoretically investigate the propagating SWs in ferromagnetic films excited by microwave fields with generic chiralities. We find that left-hand microwaves can drive SWs because of the ellipticity mismatch between microwave and dynamic magnetization, which is an extrapolation of the aforementioned selection rule for magnon-photon conversion. Since the contributions of the in-plane and out-of-plane components of left- (right-) hand microwave fields are destructive (constructive) when superposed, we introduce an analog to the common and differential signals in the differential amplifier. Surprisingly, we find a compensation frequency where no SWs can be excited by left-hand microwaves with a certain ellipticity. We propose a proof-of-concept strategy for generating nonreciprocal SWs by applying the left-hand local microwave unevenly across the film thickness. A directional mutual demagnetizing factor is suggested to understand the emerging switchable SW chirality that depends on the microwave frequency. This proposal makes full use of the magnetic structures without breaking the symmetry of the dispersion relations and increasing the damping. Our work lays the foundation for employing chiral excitation for magnonic diodes at nanoscales.

*Corresponding author: yan@uestc.edu.cn

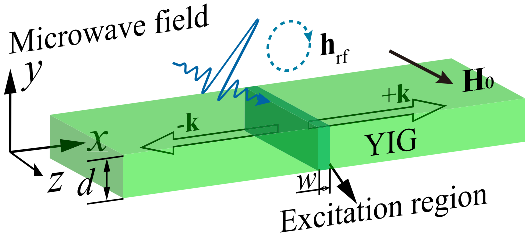

FIG. 1. Schematic of the chiral excitation of SWs. The microwave field $\mathbf{h}_{\rm rf}$ is locally applied in the deep green region. The SWs are propagating along the x direction, indicated by the hollow arrows.

This paper is organized as follows. In Sec. II, we present the characteristics of the chiral excitation of SWs via a combination of theoretical analysis and numerical simulations. The strategy for nonreciprocal SW excitations is proposed and demonstrated in Sec. III. Conclusions are drawn in Sec. IV.

II. CHARACTERISTICS OF SPIN WAVES DRIVEN BY CHIRAL EXCITATIONS

A. Modeling and dispersion relation

We consider a YIG layer with thickness d extended in the x-z plane and magnetized along the z direction by the bias magnetic field $\mathbf{H}_0 = H_0\mathbf{z}$ (see Fig. 1). The microwave field $\mathbf{h}_{\rm rf}$ for the SW excitation is centered at $x = 0$ and located in the region with width w. The characteristics of SWs propagating along the x direction, i.e., the DE geometry [16], are explored. In the calculations, we set $d = 40$ nm, $H_0 = 52$ mT, and $w = 10$ nm if not stated otherwise. The narrow excitation width ensures $\mathbf{h}_{\rm rf}$ comprises multiple wave vectors in a wide range covering those of studied SWs [54,64]. Micromagnetic simulations are performed using MUMAX3 [65] to verify the analytical results. The systems are meshed by cells with dimensions $2 \times 2 \times 100\ \mathrm{nm}^3$. Periodic boundary conditions (PBC) are applied to simulate the practically infinite film in the z direction. Absorbing boundary conditions are applied by adding the attenuating areas (not shown in Fig. 1) where α gradually increases to 0.25 to avoid the reflection at both the left and right ends of simulated systems.

The magnetization dynamics is governed by the Landau-Lifshitz-Gilbert equation

$$\frac{\partial \mathbf{M}}{\partial t} = -\gamma\mu_0\mathbf{M}\times\mathbf{H}_{\rm eff} + \frac{\alpha}{M_s}\mathbf{M}\times\frac{\partial \mathbf{M}}{\partial t}, \tag{1}$$

where γ is the gyromagnetic ratio; μ_0 is the vacuum permeability; $\alpha \ll 1$ is the dimensionless Gilbert damping constant; M_s is the saturated magnetization; $\mathbf{M} = \mathbf{m} + M_s\mathbf{z}$ is the magnetization, with $\mathbf{m} = m_x\mathbf{x} + m_y\mathbf{y}$ being the dynamic component; and $\mathbf{H}_{\rm eff} = \mathbf{H}_0 + \mathbf{h}_{\rm rf} + \mathbf{h}_{\rm ex} + \mathbf{h}_d$, with $\mathbf{h}_{\rm rf} = h_x\mathbf{x} + h_y\mathbf{y}$ being the microwave field, $\mathbf{h}_{\rm ex} = (2A_{\rm ex}/\mu_0M_s^2)\nabla^2\mathbf{m}$ being the exchange field, where $A_{\rm ex}$ is the exchange constant, and $\mathbf{h}_d$ being the dipolar field satisfying the magnetostatic Maxwell's equations $\nabla\cdot(\mathbf{h}_d + \mathbf{m}) = 0$ and $\nabla\times\mathbf{h}_d = 0$. The magnetic parameters of YIG are $M_s = 1.48 \times 10^5$ A/m, $A_{\rm ex} = 3.1 \times 10^{-12}$ J/m, and $\alpha = 5 \times 10^{-4}$ [64]. The free boundary conditions at the top and bottom surfaces require $\partial m_{x(y)}/\partial y|_{y=0,-d} = 0$ [66]. Thus, only the first unpinned mode with the mode profile being uniform across the thickness, exists in the low-frequency band due to the ultrathin thickness [34,67]. We assume a plane-wave form $\mathbf{m} = \mathbf{m}_0e^{j(\omega t - k_x x)}$, with $\mathbf{m}_0 = m_{x0}\mathbf{x} + m_{y0}\mathbf{y}$ and $m_{x(y)} = m_{x0(y0)}e^{j(\omega t - k_x x)}$. Substituting these terms into Eq. (1) and adopting the linear approximation [68], we obtain

$$j\omega m_x + (j\alpha\omega + \omega_y)m_y = \omega_M h_y, \tag{2a}$$

$$-(j\alpha\omega + \omega_x)m_x + j\omega m_y = -\omega_M h_x, \tag{2b}$$

where $\omega_x = n_x\omega_M + \omega_H + \omega_{\rm ex}$ and $\omega_y = n_y\omega_M + \omega_H + \omega_{\rm ex}$, with $\omega_M = \gamma\mu_0M_s$, $\omega_H = \gamma\mu_0H_0$, and $\omega_{\rm ex} = (2\gamma A/M_s)k_x^2$. The demagnetizing factors n_x and n_y in $\mathbf{h}_d = -n_xm_x\mathbf{x} - n_ym_y\mathbf{y}$ are given by (see Sec. A 1 for a detailed derivation)

$$n_x = 1 - n_y = 1 - \frac{1 - e^{-|k_x|d}}{|k_x|d}. \tag{3}$$

The nonzero m_x and m_y in Eqs. (2) require a vanishing determinant of the coefficient matrix, which gives a dispersion relation without considering the damping

$$\omega = \sqrt{\omega_x\omega_y}. \tag{4}$$

To verify the theoretical dispersion relation, we perform the micromagnetic simulation in the YIG film with the length of 50 μm. We consider a sinc function $\mathbf{h}_{\rm rf}(t) = h_0\sin[\omega_f(t - t_0)]/[\omega_f(t - t_0)]\mathbf{x}$, with the cutoff frequency $\omega_f/2\pi = 50$ GHz, $t_0 = 0.5$ ns, and $h_0 = 1$ mT. The total simulation time is 200 ns. The dispersion relations were obtained using the two-dimensional fast Fourier transform operation on m_y/M_s [69]. The SW dispersion relation obtained from the simulation shows good agreement with the analytical formula, as shown in Fig. 2(a). Particularly, only one band exists in the low-frequency range from 3 to 8 GHz, whose profile across the thickness is uniform, as shown in the inset of Fig. 2(a), thus justifying our analysis.

B. Ellipticity of spin precession

By solving Eqs. (2), we obtain

$$m_x = \chi_y(k_x,\omega)h_x + j\kappa(k_x,\omega)h_y, \tag{5a}$$

$$m_y = -j\kappa(k_x,\omega)h_x + \chi_x(k_x,\omega)h_y, \tag{5b}$$

where

$$\chi_x(k_x,\omega) = -\frac{(\omega_x + j\alpha\omega)\omega_M}{\omega^2 - (\omega_x + j\alpha\omega)(\omega_y + j\alpha\omega)}, \tag{6a}$$

$$\chi_y(k_x,\omega) = -\frac{(\omega_y + j\alpha\omega)\omega_M}{\omega^2 - (\omega_x + j\alpha\omega)(\omega_y + j\alpha\omega)}, \tag{6b}$$

$$\kappa(k_x,\omega) = -\frac{\omega\omega_M}{\omega^2 - (\omega_x + j\alpha\omega)(\omega_y + j\alpha\omega)}. \tag{6c}$$

The coefficients $\chi_x(k_x,\omega)$, $\chi_y(k_x,\omega)$, and $\kappa(k_x,\omega)$ possess the same denominator, whose absolute value takes the minimum when the dispersion relation (4) is satisfied. This means that even though the microwave field comprises multiple wave vector components within $2\pi/w$ [54,64], only SWs with k_x and ω satisfying Eq. (4) can be efficiently excited. Substituting

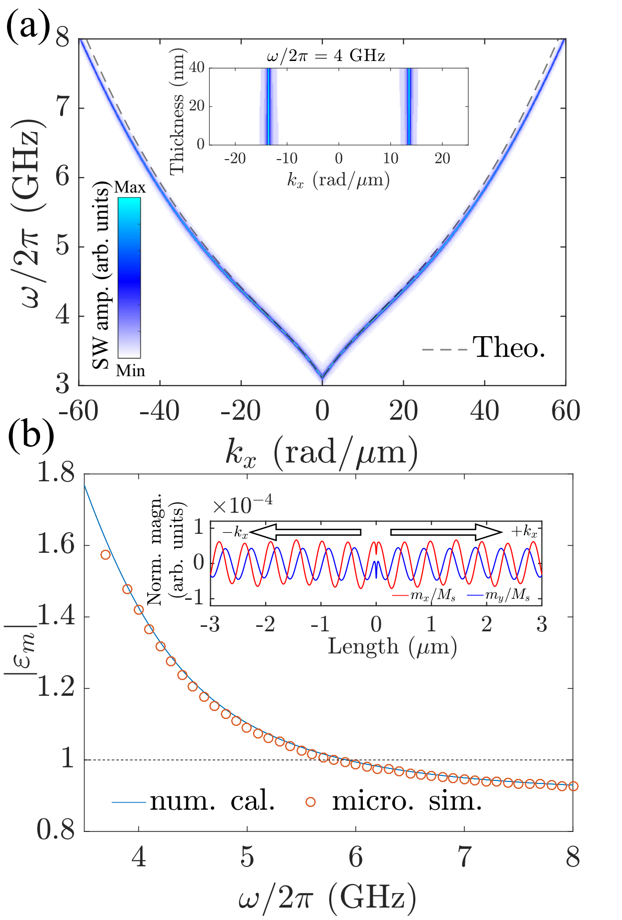

FIG. 2. (a) SW dispersion relation for the film obtained from micromagnetic simulations. The dashed line represents the theoretical result from Eq. (4). Inset: Profiles of SWs with various wave vectors across the thickness at 4 GHz. (b) Frequency dependence of the dynamic magnetization ellipticity $|\varepsilon_m|$. The solid curve is from Eq. (9). Circles are micromagnetic simulations. The dashed line indicates $|\varepsilon_m| = 1$. Inset: Spatial distribution of normalized dynamic magnetization $m_{x(y)}/M_s$ at 4 GHz at an arbitrary time. The blue (red) curve represents the x (y) component.

Eq. (4) into Eqs. (6) and neglecting higher-order terms, the magnetic parameters reduce to

$$m_x = \chi_y h_x + j\kappa h_y, \tag{7a}$$

$$m_y = -j\kappa h_x + \chi_x h_y, \tag{7b}$$

with

$$\chi_x = -\frac{j\omega_x\omega_M}{\alpha(\omega_x + \omega_y)\sqrt{\omega_x\omega_y}}, \tag{8a}$$

$$\chi_y = -\frac{j\omega_y\omega_M}{\alpha(\omega_x + \omega_y)\sqrt{\omega_x\omega_y}}, \tag{8b}$$

$$\kappa = -\frac{j\omega_M}{\alpha(\omega_x + \omega_y)}. \tag{8c}$$

We obtain the ratio between the x and y components of the dynamic magnetization as

$$\varepsilon_m = \frac{m_x}{m_y} = j\sqrt{\frac{\omega_y}{\omega_x}} = j\sqrt{\frac{n_y\omega_M + \omega_H + \omega_{\text{ex}}}{n_x\omega_M + \omega_H + \omega_{\text{ex}}}}. \tag{9}$$

Equation (9) indicates the following features of spin precessions: (i) the imaginary unit j in ε_m implies spin precessions in ferromagnetic films are always right-handed, as shown in the inset of Fig. 2(b), where m_y drops behind m_x for 1/4 of the wavelength regardless of their propagating directions. (ii) ε_m is irrelevant to the amplitude or phase of h_x and h_y. In the limit of $k_x \to \infty$, we have $\varepsilon_m \to j$ indicating that exchange SWs are perfectly right-handed [70]. Meanwhile, in the dipolar-exchange region, ε_m varies with factors n_x and n_y. The frequency dependence of $|\varepsilon_m|$ is shown in Fig. 2(b).

C. Intensity spectra

Below, we investigate the dependence of SW amplitudes $|\mathbf{m}| = \sqrt{m_x^2 + m_y^2}$ on the microwave field chirality. Specifically, we inspect the typical case in which $\varepsilon_h = h_x/h_y$ is purely imaginary, where $h_x = j|\varepsilon_h|h_y$ and $h_x = -j|\varepsilon_h|h_y$ represent, respectively, the right- and left-handed polarizations, with $|\varepsilon_h|$ being their ellipticity. In micromagnetic simulations, the excitation is applied using the function $\mathbf{h}_{\text{rf}}(t) = h_{x0}\sin(\omega t)\mathbf{x} + h_{y0}\sin(\omega t \pm \pi/2)\mathbf{y}$, with $+$ ($-$) indicating the left- (right-) hand polarization. We fix $h_0 = \sqrt{h_{x0}^2 + h_{y0}^2} = 0.1$ mT to ensure the same rf power density with different ellipticities. The results spatiotemporally record the evolution of the dynamic normalized magnetization (m_x/M_s and m_y/M_s). The amplitude spectra of the SWs excited by the right- and left-hand polarized microwaves with $|\varepsilon_h|$ ranging from 0.9 to 1.1 are plotted in Figs. 3(a) and 3(b), respectively.

The chiral excitation of SWs has the following features. First, the complex parameters χ_x, χ_y, and κ expressed by Eqs. (8) take the same phase factor. Therefore, Eqs. (7) indicate that the contribution of h_y to $\mathbf{m}$ is delayed by the phase of $\pi/2$ compared to that of h_x. Consequently, the contributions of h_x and h_y are superposed destructively (constructively) in the case of left- (right-) hand excitation. We thus introduce an analog to the differential amplifier in electronic systems, in which the dual inputs are separately amplified, then subtracted (added), and, finally, output as different (common) mode signals [71], as illustrated by the insets in Figs. 3(a) and 3(b). The dual inputs, amplifying factors, and outputs should be compared with $\mathbf{h}_{\text{rf}}$, the complex parameters (χ_x, χ_y or κ), and $\mathbf{m}$, respectively. And ε_h reflects the ratio between the dual inputs. Substituting $h_x = j|\varepsilon_h|h_y$ and $h_x = -j|\varepsilon_h|h_y$ into Eqs. (7), we obtain

$$\begin{bmatrix} m_x \\ m_y \end{bmatrix} = \begin{bmatrix} jh_y(\kappa \pm |\varepsilon_h|\chi_y) \\ h_y(\chi_x \pm |\varepsilon_h|\kappa) \end{bmatrix}, \tag{10}$$

with $+$ and $-$ indicating the results of right- and left-handed excitations, respectively, which justifies the analog to the differential amplifier model.

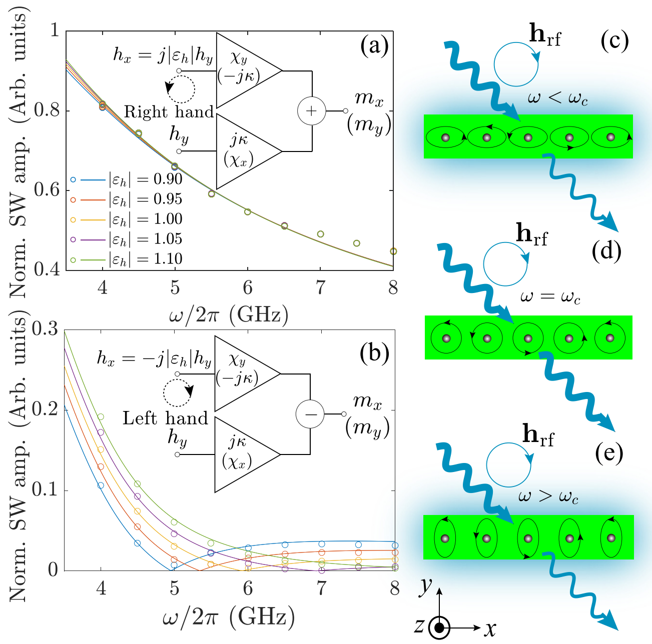

FIG. 3. SW amplitudes $|\mathbf{m}|$ normalized by the maximal value excited by (a) the right- and (b) left-hand chiral microwave fields with the same power density but different ellipticities ranging from 0.9 to 1.1. Solid curves are calculated based on Eqs. (7). Insets in (a) and (b) depict the schematics of constructive and destructive superpositions of the contributions of h_x and h_y, analogous to the common and different signals in differential amplifiers, respectively. Symbols are from micromagnetic simulations. Illustrations of the left-hand chiral photon-magnon conversion (c) below, (d) at, and (e) above ω_c. The blue wavy arrays and circles represent the microwave fields, with thickness indicating the intensity, where the blue arrowed circles represent the microwave chirality. The blue shaded backgrounds indicate the converted microwave energy. The dots and circles represent the spins and their precession cones, respectively.

Second, using the differential amplifier model, it can be explained that the left-hand excited SW spectra are much more sensitive to the variation of ε_h than the right-hand excited ones since the differential (common) mode signal is sensitive (insensitive) to the variation ε_h of the dual inputs (h_x and h_y). It is observed that curves describing different ε_h in Fig. 3(a) almost merge, while those in Fig. 3(b) are well separated. Moreover, the intensity of left-hand excited SWs is much weaker than that of their right-hand counterparts. Especially, the former drops to almost one tenth of the latter at high frequencies.

Last, even though the two pairs of amplifying factors [(χ_y, κ) and (κ, χ_x)] for the outputs m_x and m_y are different, their ratios are both $1/|\varepsilon_m|$. Mathematically, we can substitute Eqs. (8) and (9) into Eqs. (7) and obtain

$$\begin{bmatrix} m_x \\ m_y \end{bmatrix} = -\frac{\omega_m h_y(\varepsilon_h\varepsilon_m - 1)}{\alpha(\omega_x + \omega_y)}\begin{bmatrix} 1 \\ 1/\varepsilon_m \end{bmatrix}. \tag{11}$$

It suggests a compensation frequency ω_c when $\varepsilon_h\varepsilon_m = 1$. Equation (9) indicates $\mathrm{Im}(\varepsilon_m) > 0$; therefore, only the left-hand microwaves with $\mathrm{Im}(\varepsilon_h) < 0$ support ω_c, at (below and above) which the microwave with any intensity is unable (able) to excite any SWs, as illustrated in Figs. 3(c), 3(d), and 3(e). The equality of the ratios is also a prerequisite for treating SWs as scalar variables in previous studies [72–74]. This finding broadens the selection rule for photon-magnon conversion, which is instructive for the chiral magneto-optic and -acoustic effects [30,75]. However, ω_c cannot exist for arbitrary ε_h because $|\varepsilon_m|$ given by Eq. (9) can take a value only from 0.91 to 2.14 for the present model parameters. Consequently, ω_c can emerge with $|\varepsilon_h|$ only in the range from 0.47 to 1.09. Analytical and numerical results indeed verify this point that the curve for $|\varepsilon_h| = 1.1$ (the green one) in Fig. 3(b) cannot intersect with the x axis.

III. STRATEGY FOR NONRECIPROCAL SPIN WAVES

Typically, propagating SWs in single DMI-free nanometer-thick films are weakly nonreciprocal, because the DE mechanism requires the film thickness to be comparable to the wavelengths of SWs for prominent nonreciprocity [16,17]. The above discussions indicate that using the left-hand excitation is essential to enhance the nonreciprocity due to the high sensitivity of the SW spectra to ε_h. We need to only slightly alter the ellipticity (ε_h^+ and ε_h^-) of the microwave fields to excite the forward and backward propagating SWs with quite different spectra (superscripts + and − are used to label the forward and backward parameters, respectively, hereinafter). In comparison, the right-hand excitation case requires ε_h^+ and ε_h^- to vary dramatically for substantially different spectra. Hence, the left-handed excitation brings a great convenience for designing a method for nonreciprocity. One critical technique is to differentiate ε_h^+ and ε_h^-. In the multilayer structure, the dynamic mutual dipolar effect between layers has been demonstrated to be directionally dependent [76]. So a natural issue arises if we can introduce the mutual dipolar field combined with $\mathbf{h}_{\rm rf}$ to differentiate ε_h^+ and ε_h^-. Here, we propose a method by applying microwave fields unevenly across the film thickness. This idea is in contrast to preceding works, where additional micromagnets outside YIG films were indispensable as the SW source and the polarizations of driving fields were simply circular with directionally opposite chiralities, resulting in the nonreciprocity [50,51,62,63,70]. For simplicity, we consider a left-handed $\mathbf{h}_{\rm rf}$ with $|\varepsilon_h| = 1$ uniformly applied only to the top part of the film with thickness d_1 and width w, as shown in Fig. 4(a). The SW information in the excitation area along the thickness is extracted by calculating $|\mathbf{m}|$ at every mesh grid, and is averaged and normalized. We evaluate the dynamic magnetizations ($\mathbf{m}_1 = m_{x,1}\mathbf{x} + m_{y,1}\mathbf{y}$ and $\mathbf{m}_2 = m_{x,2}\mathbf{x} + m_{y,2}\mathbf{y}$) along d_1 and $d_2 = d - d_1$ that introduce the mutual demagnetizing field, with the simulated SW amplitudes shown in Fig. 4(b). Even though a minor inhomogeneity appears at the interface, the SW is treated to be transversely uniform in each part in the following analysis. The part in the dashed red box with a bilayer structure is regarded as the SW source. In this case, the dipolar fields are composed of two components: the self-demagnetizing field $\mathbf{h}_{d,p} = -n_{x,p}m_{x,p}\mathbf{x} - n_{y,p}m_{y,p}\mathbf{y}$, where $n_{x(y),p}$ is given by Eq. (3), with $n_{x(y)} \to n_{x(y),p}$ and $d \to d_p$, and the mutual demagnetizing field $\mathbf{h}_{d,pq} = h_{d,x,pq}\mathbf{x} +$

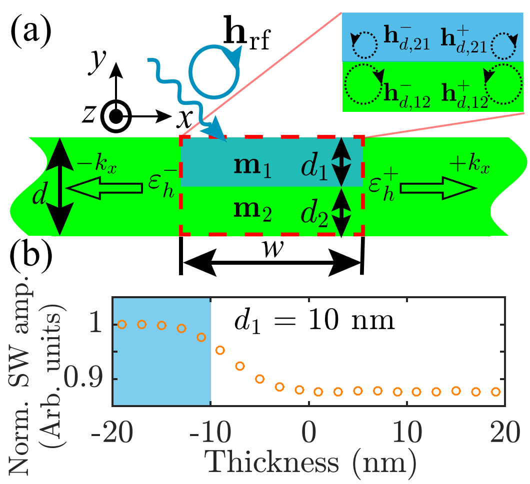

FIG. 4. (a) The schematic for the nonreciprocal SW excitation using left-hand chiral microwave field applied to the top part of the film in the blue area. The inset shows the precession cones of the mutual dipolar fields induced by the forward and backward propagating SWs in each layer, with the amplitude indicated by the radius. (b) Simulated SW amplitudes in the red box for $d_1 = 10$ nm at 4.6 GHz.

$h_{d,y,pq}\mathbf{y}$ $[(p, q) = (1, 2)$ or $(2, 1)]$. Here, $h_{d,x(y),pq}$ satisfies the following identity (see Sec. A 2 for detailed derivation):

$$\begin{bmatrix} h_{d,x,pq} \\ h_{d,y,pq} \end{bmatrix} = -n_{pq} \begin{bmatrix} 1 & j\mathrm{sgn}(k_x)(q-p) \\ j\mathrm{sgn}(k_x)(q-p) & -1 \end{bmatrix} \begin{bmatrix} m_{x,p} \\ m_{y,p} \end{bmatrix}, \tag{12}$$

with

$$n_{pq} = \frac{(1 - e^{-|k_x|d_p})(1 - e^{-|k_x|d_q})}{2|k_x|d_q}. \tag{13}$$

$\mathbf{h}_{d,pq}$ ($\mathbf{h}_{d,p}$) is directionally dependent (independent) according to Eqs. (12) [Eq. (3)]. Hence, $\mathbf{h}_{d,pq}$ rather than $\mathbf{h}_{d,p}$ contributes to the nonreciprocity. In addition, $\mathbf{h}^+_{d,21}$ ($\mathbf{h}^-_{d,21}$) and $\mathbf{h}^+_{d,12}$ ($\mathbf{h}^-_{d,12}$) are oppositely circularly polarized with different intensities, as sketched in the inset of Fig. 4(a) [see Eqs. (A27) in Sec. A 2]. The net effective mutual field $\mathbf{h}_{d,\mathrm{mut}}$ for the entire film is therefore given by

$$\begin{aligned} \mathbf{h}_{d,\mathrm{mut}} &= \frac{\mathbf{h}_{d,12}d_2 + \mathbf{h}_{d,21}d_1}{d} \\ &= -n_{\mathrm{mut}}\{[(m_{x,1} + m_{x,2}) + j\mathrm{sgn}(k_x)(m_{y,1} - m_{y,2})]\mathbf{x} \\ &\quad + [j\mathrm{sgn}(k_x)(m_{x,1} - m_{x,2}) - (m_{y,1} + m_{y,2})]\mathbf{y}\}, \end{aligned} \tag{14}$$

with

$$n_{\mathrm{mut}} = \frac{(1 - e^{-|k_x|d_1})(1 - e^{-|k_x|d_2})}{2|k_x|d}. \tag{15}$$

Following conclusions can thus be drawn. First, the nonreciprocity disappears if $d_1 = 0$ or $d_2 = 0$, which causes $n_{\mathrm{mut}} = 0$ and $\mathbf{h}_{d,\mathrm{mut}} = 0$. It was confirmed that SWs propagating along opposite directions have the same amplitude as the uniform excitation across the thickness, as shown in Fig. 2(b). Second, since $\mathbf{h}_{d,\mathrm{mut}}$ is determined by $\mathbf{m}_1$ and $\mathbf{m}_2$, its role is to tune the two gains in the differential amplifier [see insets of Figs. 3(a) and 3(b)], equivalent to varying ε_h of the input microwave $\mathbf{h}_{\mathrm{rf}}$. As the variation of ε_h is directional with $\mathbf{h}_{d,\mathrm{mut}}$, the intensity spectra are well separated for the forward and backward SWs, as plotted in Fig. 5(a). It is noted that the strength of $\mathbf{h}_{\mathrm{rf}}$ is typically one order of magnitude stronger than $\mathbf{h}_{d,\mathrm{mut}}$, such that the effective mutual field can modify the ellipticity of the external left-handed microwave by 10% [see the inset of Fig. 5(a)]. This modification is sufficient to generate a significant non-reciprocity because of the high sensitivity of the left-handed microwave to its ellipticity. Even though $\mathbf{h}_{d,\mathrm{mut}}$ is frequency dependent, simulation results can still be well fitted using Eqs. (7) and $h_x = \varepsilon_h^{+(-)}(d_1)h_y$, with ω_c satisfying $\varepsilon_h^{+(-)}(d_1)\varepsilon_m = 1$, where $\varepsilon_h^{+(-)}(d_1)$ is the effective ellipticity to be determined. The fitted $|\varepsilon_h^{+(-)}(d_1)|$ is plotted in the inset of Fig. 5(a), where the goodness of all fittings is greater than 91%. Representatively, we obtain $|\varepsilon_h^+(10\ \mathrm{nm})| = 1.05$ and $|\varepsilon_h^-(10\ \mathrm{nm})| = 0.93$, corresponding to $\omega_c/2\pi = 5.1$ and 6.7 GHz, with the dynamic magnetization presented in upper and lower panels of Fig. 5(b), respectively. Sacrificing the efficiency of excitations with the amplitude being one order lower than that in the inset of Fig. 2(b), we obtain theoretically switchable nonreciprocities and 100% (perfect) unidirectionality. This is advantageous over many other strategies [75]. Third, the difference between ε_h^+ and ε_h^- and the separation of the forward and backward SW intensity spectra approach the maximum at $d_1 = d_2 = d/2$, meeting the maximal value condition of n_{mut} in Eq. (15). However, the value of $|\varepsilon_h^+(d_1 = 20\ \mathrm{nm})| = 1.13$ exceeds the range from 0.47 to 1.09. This indicates that no ω_c would be present in the forward SW spectra, as discussed in Sec. II C. Consequently, perfect backward SW propagation without any forward SW cannot be achieved in such a case.

Last, for completeness, we perform simulations by applying right-handed and lineally polarized microwaves to the top part of the films with $d_1 = 10$ nm. Both forward and backward SWs are present, as shown in Fig. 5(c). Following features are observed. (i) Both spectra are not well separated, indicating that $\mathbf{h}_{d,\mathrm{mut}}$ can induce the nonreciprocity, but the effect is not significant. The insignificant nonreciprocity can be understood in this configuration since ferromagnetic films are much thinner than the SW length [62,63]. (ii) The forward SWs are always stronger than the backward ones in the whole frequency band, implying that the DE mechanism induced nonreciprocity cannot be switched by tuning frequencies since it is merely dependent on the surface normal and static magnetization directions [18,19]. In conclusion, switchable and perfect nonreciprocities do not appear in the spectra of right-hand and linear excitations, verifying that the left-hand excitation can cooperatively enhance, and even modify the nonreciprocity induced by $\mathbf{h}_{d,\mathrm{mut}}$.

Finally, we note that the key to exciting nonreciprocal SWs is the nonzero $\mathbf{h}_{d,\mathrm{mut}}$, induced by $\mathbf{m}$ that is asymmetrically distributed across the film thickness, which can be simply excited by an unevenly profiled $\mathbf{h}_{\mathrm{rf}}$. Such fields can be generated by resonant spin nano-oscillators with various structures, like nanodisks [77] and nanowires [78]. It is noted that $\mathbf{h}_{\mathrm{rf}}$ with more gradually uneven profiles can also excite nonreciprocal SWs. To verify this point, we performed simulations using left-handed $\mathbf{h}_{\mathrm{rf}}$ with exponential-

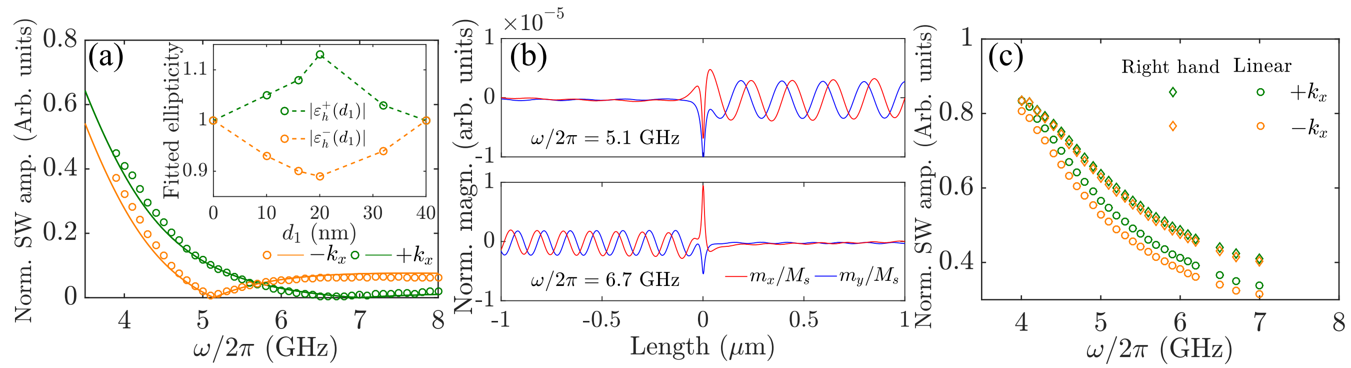

FIG. 5. (a) Spectra of the forward (green) and backward (orange) SW amplitudes with excitation depths $d_1 = 20$ nm. The intensities are normalized with the maximal value. Symbols are numerical simulations, and the curves are fitting results. The inset of (a) shows the fitted ε_h^+ and ε_h^- dependence on d_1. (b) Simulated m_x/M_s and m_y/M_s distributions at two compensation frequencies, $\omega/2\pi = 5.1$ and 6.7 GHz. (c) Simulated forward (green symbols) and backward (orange symbols) SW spectra under the right-hand (diamonds) and linear (circles) excitations unevenly applied across the film thickness ($d_1 = 10$ nm).

decaying profiles and $|\varepsilon_h| = 1$, as shown in the inset of Fig. 6. The dependence of the intensity on the thickness is described by $h_0(y) = h_0(\lambda)e^{-y/\lambda}$, where $h_0(\lambda)$ is determined by $\int_{-d}^{0} h_0(y)dy = h_0 d$ ($h_0 = 0.1$ mT) to ensure the same power intensity. The ratio $|\mathbf{m}^-|/|\mathbf{m}^+|$, which depends on the decay length λ, is plotted in Fig. 6. When λ is shorter than d, the ratio increases dramatically with the increase of λ due to the rapid decrease of the uneven degree of the exciting field. It converges to 100% with $\lambda \to \infty$, demonstrating the absence of the nonreciprocity. We point out that the switched nonreciprocity at two compensation frequencies contributes an additional methodology for magnonic frequency division multiplexing, broadening the strategy for designing magnonic circuits [79].

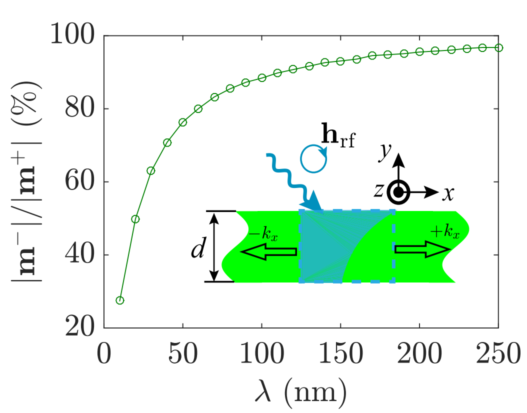

FIG. 6. Simulated $|\mathbf{m}^-|/|\mathbf{m}^+|$ dependence on the decay length of the exponential profile left-handed excitations at 4.6 GHz. The line connecting the symbols guides the trend. The inset schematically shows the simulated structure with $d = 40$ nm. The microwave field is applied to the dashed area with the exponential intensity profile indicated by the blue area.

IV. CONCLUSION

In summary, we investigated the propagating dipolar-exchange SWs excited by chiral microwaves in ferromagnetic thin films. We showed that the left-hand microwave can excite nonreciprocal SWs in the presence of ellipticity mismatch. When the left-hand microwave was unevenly applied across the film thickness, we observed a SW chirality switching by tuning the microwave frequency. Our findings shine a light on the photon-magnon conversion and pave the way toward engineering the nanoscale chiral microwave field for the realization of diodelike functionalities in magnonics.

ACKNOWLEDGMENTS

We thank Y. Henry for helpful discussions. This work was funded by the National Key Research Development Program under Contract No. 2022YFA1402802 and the National Natural Science Foundation of China (NSFC; Grants No. 12074057, No. 11604041, and No. 11704060). Z.Z. acknowledges financial support from the China Postdoctoral Science Foundation under Grant No. 2020M673180. Z.W. was supported by the China Postdoctoral Science Foundation under Grant No. 2019M653063 and the NSFC (Grant No. 12204089). Z.-X.L. acknowledges financial support from the China Postdoctoral Science Foundation (Grant No. 2019M663461) and the NSFC (Grant No. 11904048).

APPENDIX

We investigate the dipolar effect induced by SWs propagating in an ultrathin magnetic film. The dipolar field in the whole space is calculated. The self- and mutual demagnetizing factors are figured out in Secs. A 1 and A 2, respectively. We considered a magnetic film extended infinitely along the x and z directions, located from $y = -d$ to 0 and labeled L_i. The SWs take the form $\mathbf{m}_i = \mathbf{m}_{0,i}e^{j(\omega t - k_x x)} = m_{x,i}\mathbf{x} + m_{y,i}\mathbf{y}$,

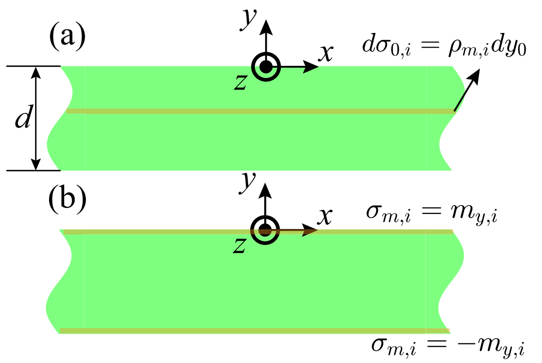

FIG. 7. Schematics of the effective (a) *volume* and (b) *surface* magnetic charges. The yellow parts represent the differential elements.

with $\mathbf{m}_{0,i} = m_{x0,i}\mathbf{x} + m_{y0,i}\mathbf{y}$. The dynamic magnetization $\mathbf{m}_i$ and the dipolar field $\mathbf{h}_{d,i}$ satisfy the magnetostatic equations

$$\nabla \cdot (\mathbf{h}_{d,i} + \mathbf{m}_i) = 0, \tag{A1a}$$

$$\nabla \times \mathbf{h}_{d,i} = 0. \tag{A1b}$$

By introducing the scale potential $\psi_{m,i}$, we have

$$\mathbf{h}_{d,i} = -\nabla \psi_{m,i}. \tag{A2}$$

Then Eq. (A1a) becomes the Poisson equation

$$\nabla^2 \psi_{m,i} = -\rho_i, \tag{A3}$$

where ρ_i is the effective magnetic-charge density,

$$\rho_i = -\nabla \cdot \mathbf{m}_i. \tag{A4}$$

One crucial step is to find the solution of $\psi_{m,i}$ in Eq. (A3). We note that there are two contributions to $\psi_{m,i}$ in magnetic materials: the effective *volume* magnetic-charge density $\rho_{m,i}$ and the effective *surface* magnetic-charge density $\sigma_{m,i}$ [80].

First, we calculate the contribution of $\rho_{m,i}$. Inside the film, $\rho_{m,i} = -\nabla \cdot \mathbf{m}_i = jk_x m_{x,i}$ is induced by the x component of m_i [76]. To begin, we consider a tiny sheet of a film located at position $y = y_0$ with thickness dy_0, whose surface magnetic charge density is $\sigma_{0,i} = \rho_{m,i} dy_0$ [see Fig. 7(a)]. The magnetostatic potential $\psi_{m,i}(\sigma_{0,i}, y_0, \mathbf{r}, t)$ induced by $\sigma_{0,i}$ is periodic (evanescent) along the x (y) direction, while its maximum locates at $y = y_0$ and satisfies the Laplace equation $\nabla^2 \psi_{m,i}(\sigma_{0,i}, y_0, \mathbf{r}, t) = 0$ [81]. Then the solution can be expressed as

$$\psi_{m,i}(\sigma_{0,i}, y_0, \mathbf{r}, t) = \psi_{m0,i}(\sigma_{0,i}) e^{-|k_x(y-y_0)|} e^{j(\omega t - k_x x)}. \tag{A5}$$

The next step is to find the value of $\psi_{m0,i}$. Note that the boundary condition (continuity of B_y) of the tiny sheet is given as

$$h_{y,i}(\sigma_{0,i}, y_0^+, \mathbf{r}, t) - h_{y,i}(\sigma_{0,i}, y_0^-, \mathbf{r}, t) = \sigma_{0,i}. \tag{A6}$$

Using Eq. (A2), we have

$$\begin{aligned} h_{y,i}(\sigma_{0,i}, y_0, \mathbf{r}, t) &= -\frac{\partial}{\partial y}\psi_{m,i}(\sigma_{0,i}, y_0, \mathbf{r}, t) \\ &= \begin{cases} |k_x|\psi_{m0,i} e^{|k_x|(y-y_0)} e^{j(\omega t - k_x x)}, & y \geqslant y_0, \\ |k_x|\psi_{m0,i} e^{-|k_x|(y-y_0)} e^{j(\omega t - k_x x)}, & y < y_0. \end{cases} \end{aligned} \tag{A7}$$

Therefore, we have

$$2|k_x|\psi_{m0,i}(\sigma_{0,i}) e^{j(\omega t - k_x x)} = \sigma_{0,i}. \tag{A8}$$

The magnetostatic potential induced by the sheet at $y = y_0$ can be expressed as

$$\psi_{m,i}(\sigma_{0,i}, y_0, \mathbf{r}, t) = \frac{j\mathrm{sgn}(k_x) m_{x0,i} e^{j(\omega t - k_x x)}}{2} e^{-|k_x(y-y_0)|} dy_0. \tag{A9}$$

Therefore, the dipolar magnetic field $\mathbf{h}_{d,i}(\sigma_{0,i}, y_0, \mathbf{r}, t)$ derived from $\psi_{m,i}(\sigma_{0,i}, y_0, \mathbf{r}, t)$ is given by

$$\begin{aligned} &\mathbf{h}_{d,i}(\sigma_{0,i}, y_0, \mathbf{r}, t) \\ &= \frac{j\mathrm{sgn}(k_x) m_{x,i}}{2} e^{-|k_x(y-y_0)|}[-\mathrm{sgn}(k_x)\mathbf{x} + j\mathrm{sgn}(y - y_0)\mathbf{y}] dy_0. \end{aligned} \tag{A10}$$

The dipolar field $\mathbf{h}_{d,i}(\rho_{m,i}, \mathbf{r}, t)$ induced by $\rho_{m,i}$ at any position $\mathbf{r}$ reads

$$\begin{aligned} \mathbf{h}_{d,i}(\rho_{m,i}, \mathbf{r}, t) &= \frac{1}{2}\int_{-d}^{0} j\mathrm{sgn}(k_x) m_{x,i} e^{-|k_x(y-y_0)|}[-\mathrm{sgn}(k_x)\mathbf{x} + j\mathrm{sgn}(y - y_0)\mathbf{y}] dy_0 \\ &= \begin{cases} \frac{m_{x,i}}{2} e^{-|k_x|y}(1 - e^{-|k_x|d})[-\mathbf{x} + j\mathrm{sgn}(k_x)\mathbf{y}], & y \geqslant 0, \\ -\frac{m_{x,i}}{2}[2 - e^{-|k_x|(y+d)} - e^{|k_x|y}]\mathbf{x} + \frac{jm_{x,i}}{2}\mathrm{sgn}(k_x)[e^{|k_x|y} - e^{-|k_x|(y+d)}]\mathbf{y}, & -d \leqslant y < 0, \\ \frac{m_{x,i}}{2} e^{|k_x|y}(e^{|k_x|d} - 1)[-\mathbf{x} - j\mathrm{sgn}(k_x)\mathbf{y}], & y < -d. \end{cases} \end{aligned} \tag{A11}$$

Next, we calculate the contribution from the surface magnetic charges $\sigma_{m,i} = \mathbf{m}_i \cdot \mathbf{n}$, located only at the positions $y = 0$ and $y = -d$, with $\mathbf{n}$ being the unit vector normal to the surface. The surface magnetic charges at $y = 0$ and $y = -d$ are respectively equal to $m_{y,i} = m_{y0,i} e^{j(\omega t - k_x x)}$ and $-m_{y,i}$, where the minus sign comes from the opposite directions of the top and bottom surfaces. Following the steps from Eqs. (A5) to (A9), we obtain the magnetostatic potential induced by $\sigma_{m,i}$,

$$\psi_{m,i}(\sigma_{m,i}, 0, \mathbf{r}, t) = \frac{m_{y0,i}}{2|k_x|} e^{j(\omega t - k_x x)} e^{-|k_x y|}, \tag{A12a}$$

$$\psi_{m,i}(\sigma_{m,i}, -d, \mathbf{r}, t) = -\frac{m_{y0,i}}{2|k_x|} e^{j(\omega t - k_x x)} e^{-|k_x(y+d)|}. \tag{A12b}$$

The dipolar field $\mathbf{h}_{d,i}(\sigma_{m,i}, \mathbf{r}, t)$ induced by $\sigma_{m,i}$ at any position $\mathbf{r}$ is given by [76]

$$\mathbf{h}_{d,i}(\sigma_{m,i}, \mathbf{r}, t) = -\nabla[\psi_{m,i}(\sigma_{m,i}, 0, \mathbf{r}, t) + \psi_{m,i}(\sigma_{m,i}, -d, \mathbf{r}, t)]$$
$$= \begin{cases} \frac{m_{y,i}}{2} e^{-|k_x|y}(1 - e^{-|k_x|d})[j\mathrm{sgn}(k_x)\mathbf{x} + \mathbf{y}], & y \geqslant 0, \\ -\frac{jm_{y,i}}{2}[e^{|k_x|y} - e^{-|k_x|(y+d)}]\mathrm{sgn}(k_x)\mathbf{x} + \frac{m_{y,i}}{2}[-e^{-|k_x|(y+d)} - e^{|k_x|y}]\mathbf{y}, & -d \leqslant y < 0, \\ \frac{m_{y,i}}{2} e^{|k_x|y}(e^{|k_x|d} - 1)[-j\mathrm{sgn}(k_x)\mathbf{x} + \mathbf{y}], & y < -d. \end{cases} \tag{A13}$$

Finally, we obtain the dipolar magnetic field $\mathbf{h}_{d,i}(\mathbf{r}, t) = \mathbf{h}_{d,i}(\rho_{m,i}, \mathbf{r}, t) + \mathbf{h}_{d,i}(\sigma_{m,i}, \mathbf{r}, t)$ in the entire space,

$$\mathbf{h}_{d,i}(\mathbf{r}, t) = \begin{cases} \frac{1}{2} e^{-|k_x|y}(1 - e^{-|k_x|d})\{[-m_{x,i} + j\mathrm{sgn}(k_x)m_{y,i}]\mathbf{x} + [j\mathrm{sgn}(k_x)m_{x,i} + m_{y,i}]\mathbf{y}\}, & y \geqslant 0, \\ \left\{[e^{-|k_x|(y+d)} + e^{|k_x|y} - 2]\frac{m_{x,i}}{2} + \frac{j\mathrm{sgn}(k_x)}{2}[e^{-|k_x(y+d)|} - e^{-|k_xy|}]m_{y,i}\right\}\mathbf{x} & \\ + \left\{\frac{j\mathrm{sgn}(k_x)}{2}[e^{|k_x|y} - e^{-|k_x|(y+d)}]m_{x,i} - [e^{-|k_xy|} + e^{-|k_x(y+d)|}]\frac{m_{y,i}}{2}\right\}\mathbf{y}, & -d \leqslant y < 0, \\ \frac{1}{2} e^{|k_x|y}(e^{|k_x|d} - 1)\{[-m_{x,i} - j\mathrm{sgn}(k_x)m_{y,i}]\mathbf{x} + [-j\mathrm{sgn}(k_x)m_{x,i} + m_{y,i}]\mathbf{y}\}, & y < -d. \end{cases} \tag{A14}$$

1. Self-demagnetizing factors

When calculating the demagnetizing factor of a single layer with thickness d_i, we care about the region $-d_i < y < 0$. The demagnetizing factors inside the film are defined as the ratios between the average dipolar field and the magnetization,

$$-n_{x,i}m_{x,i} = \frac{1}{d}\int_{-d}^{0} \mathbf{x} \cdot \mathbf{h}_{d,i}(\mathbf{r}, t)dy, \tag{A15a}$$

$$-n_{yx}m_{x,i} = \frac{1}{d}\int_{-d}^{0} \mathbf{y} \cdot \mathbf{h}_{d,i}(\mathbf{r}, t)dy, \tag{A15b}$$

$$-n_{xy}m_{x,i} = \frac{1}{d}\int_{-d}^{0} \mathbf{x} \cdot \mathbf{h}_{d,i}(\mathbf{r}, t)dy, \tag{A15c}$$

$$-n_{y,i}m_{x,i} = \frac{1}{d}\int_{-d}^{0} \mathbf{y} \cdot \mathbf{h}_{d,i}(\mathbf{r}, t)dy. \tag{A15d}$$

We obtain

$$n_{x,i} = 1 - n_{y,i} = 1 - \frac{1 - e^{-|k_x|d_i}}{|k_x|d_i}, \tag{A16a}$$

$$n_{xy} = n_{yx} = 0. \tag{A16b}$$

The net self-induced dipolar field $\mathbf{h}_{d,\mathrm{self},i} = h_{d,\mathrm{self},i,x}\mathbf{x} + h_{d,\mathrm{self},i,y}\mathbf{y}$ of the SWs can be evaluated

$$\begin{bmatrix} h_{d,\mathrm{self},i,x} \\ h_{d,\mathrm{self},i,y} \end{bmatrix} = -\begin{bmatrix} n_{x,i} & 0 \\ 0 & n_{y,i} \end{bmatrix}\begin{bmatrix} m_{x,i} \\ m_{y,i} \end{bmatrix}. \tag{A17}$$

The ratio $\varepsilon_{hd,i}$ between $h_{d,\mathrm{self},i,x}$ and $h_{d,\mathrm{self},i,y}$ is given by

$$\varepsilon_{hd,i} = \frac{h_{d,\mathrm{self},i,x}}{h_{d,\mathrm{self},i,y}} = \frac{n_{x,i}m_{x,i}}{n_{y,i}m_{y,i}}, \tag{A18}$$

indicating that the chirality of the self-induced dipolar field depends on the chirality of the dynamic magnetization.

2. Mutual demagnetizing factors

In this part, we consider the dipolar effects between the two adjacent layers L_1 and L_2, as shown in Fig. 8. They are located from $y = -d_1$ to 0 and from $y = -d$ to $-d_1$, respectively. For simplicity, we denote $d_2 = d - d_1$. Propagating SWs take the form $\mathbf{m}_p = \mathbf{m}_{0,p}e^{j(\omega t - k_{x,p}x)} = m_{x,p}\mathbf{x} + m_{y,p}\mathbf{y}$, with $p = 1, 2$.

According to Eq. (A14), the dipolar field induced by $\mathbf{m}_1$ and acting on $L_2[-(d_1 + d_2) < y < -d_1]$ is given as

$$\mathbf{h}_{d,12}(\mathbf{r}, t) = \frac{1}{2}e^{|k_{x,1}|y}(e^{|k_{x,1}|d_1} - 1)\{[-m_{x,1} - j\mathrm{sgn}(k_{x,1})m_{y,1}]\mathbf{x} + [-j\mathrm{sgn}(k_{x,1})m_{x,1} + m_{y,1}]\mathbf{y}\}. \tag{A19}$$

The average dipolar field acting on L_2 can be evaluated by introducing the mutual demagnetizing factors n_{x12}, n_{xy12}, n_{yx12}, and n_{y12},

$$-n_{x12}m_{x,1} - n_{xy12}m_{y,1} = \frac{1}{d_2}\int_{-(d_1+d_2)}^{-d_1} \mathbf{x} \cdot \mathbf{h}_{d,12}(\mathbf{r}, t)dy, \tag{A20a}$$

$$-n_{yx12}m_{x,1} - n_{y12}m_{y,1} = \frac{1}{d_2}\int_{-(d_1+d_2)}^{-d_1} \mathbf{y} \cdot \mathbf{h}_{d,12}(\mathbf{r}, t)dy. \tag{A20b}$$

We thus obtain

$$n_{x12} = -n_{y12} = \frac{(1 - e^{-|k_{x,1}|d_1})(1 - e^{-|k_{x,1}|d_2})}{2|k_{x,1}|d_2}, \tag{A21a}$$

$$n_{xy12} = n_{yx12} = j\mathrm{sgn}(k_{x,1})n_{x12}. \tag{A21b}$$

The dipolar field acting on $L_1(-d_1 < y < 0)$ induced by $\mathbf{m}_2$ is given by

$$\mathbf{h}_{d,21}(\mathbf{r}, t) = \frac{1}{2}e^{-|k_{x,2}|(y+d_1)}(1 - e^{-|k_{x,2}|d_2}) \times \{[-m_{x,2} + j\mathrm{sgn}(k_{x,2})m_{y,2}]\mathbf{x} + [j\mathrm{sgn}(k_{x,2})m_{x,1} + m_{y,2}]\mathbf{y}\}. \tag{A22}$$

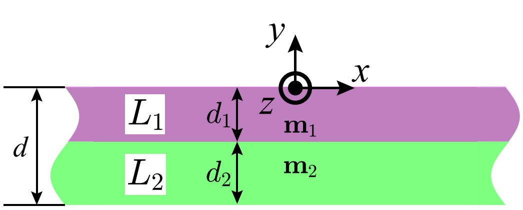

FIG. 8. Schematic of the bilayer consisting of L_1 (purple) and L_2 (green) with SWs $\mathbf{m}_1$ and $\mathbf{m}_2$ inside, respectively.

Similarly, we introduce n_{x21}, n_{xy21}, n_{yx21}, and n_{y21},

$$-n_{x21}m_{x,1} - n_{xy21}m_{y,1} = \frac{1}{d_1}\int_{-d_1}^{0} \mathbf{x}\cdot\mathbf{h}_{d,21}(\mathbf{r},t)dy, \quad \text{(A23a)}$$

$$-n_{yx21}m_{x,1} - n_{y21}m_{y,1} = \frac{1}{d_1}\int_{-d_1}^{0} \mathbf{y}\cdot\mathbf{h}_{d,21}(\mathbf{r},t)dy. \quad \text{(A23b)}$$

We thus obtain

$$n_{x21} = -n_{y21} = \frac{(1-e^{-|k_{x,2}|d_1})(1-e^{-|k_{x,2}|d_2})}{2|k_{x,2}|d_1}, \quad \text{(A24a)}$$

$$n_{xy21} = n_{yx21} = -j\mathrm{sgn}(k_{x,2})n_{x21}. \quad \text{(A24b)}$$

Finally, the mutual net dipolar fields $\mathbf{h}_{d,12} = h_{d,x,12}\mathbf{x} + h_{d,y,12}\mathbf{y}$ and $\mathbf{h}_{d,21} = h_{d,x,21}\mathbf{x} + h_{d,y,21}\mathbf{y}$ can be evaluated as

$$\begin{bmatrix} h_{d,x,12} \\ h_{d,y,12} \end{bmatrix} = -n_{x12}\begin{bmatrix} 1 & j\mathrm{sgn}(k_{x,1}) \\ j\mathrm{sgn}(k_{x,1}) & -1 \end{bmatrix}\begin{bmatrix} m_{x,1} \\ m_{y,1} \end{bmatrix} \quad \text{(A25)}$$

and

$$\begin{bmatrix} h_{d,x,21} \\ h_{d,y,21} \end{bmatrix} = -n_{x21}\begin{bmatrix} 1 & -j\mathrm{sgn}(k_{x,2}) \\ -j\mathrm{sgn}(k_{x,2}) & -1 \end{bmatrix}\begin{bmatrix} m_{x,2} \\ m_{y,2} \end{bmatrix}. \quad \text{(A26)}$$

The ratios ε_{hd12} and ε_{hd21} between $h_{d,x,12}$ and $h_{d,y,12}$ and $h_{d,x,21}$ and $h_{d,21,y}$ are given by

$$\varepsilon_{hd12} = \frac{m_{x,1} + j\mathrm{sgn}(k_{x,1})m_{y,1}}{j\mathrm{sgn}(k_{x,1})m_{x,1} - m_{y,1}} = -j\mathrm{sgn}(k_{x,1}), \quad \text{(A27a)}$$

$$\varepsilon_{hd21} = \frac{m_{x,2} - j\mathrm{sgn}(k_{x,2})m_{y,2}}{-j\mathrm{sgn}(k_{x,2})m_{x,2} + m_{y,2}} = j\mathrm{sgn}(k_{x,2}), \quad \text{(A27b)}$$

indicating that the chirality of the mutual dipolar field depends on the signs of the wave vectors. The net mutual demagnetizing field can be estimated as

$$\begin{aligned}\mathbf{h}_{d,\mathrm{mut}} &= \frac{\mathbf{h}_{d,12}d_2 + \mathbf{h}_{d,21}d_1}{d} \\ &= -\frac{(1-e^{-|k_{x,2}|d_1})(1-e^{-|k_{x,2}|d_2})}{2|k_x|d} \\ &\quad \times \{[(m_{x,1}+m_{x,2}) + j\mathrm{sgn}(k_x)(m_{y,1}-m_{y,2})]\mathbf{x} \\ &\quad + [j\mathrm{sgn}(k_x)(m_{x,1}-m_{x,2}) - (m_{y,1}+m_{y,2})]\mathbf{y}\}.\end{aligned} \quad \text{(A28)}$$

Here, we note that in the main text, the dynamic magnetizations $\mathbf{m}_1$ and $\mathbf{m}_2$ satisfy the boundary condition $\mathbf{m}_1 = \mathbf{m}_2|_{y=-d_1}$ [82], which gives $k_{x,1} = k_{x,2} = k_x$.

[1] A. Barman *et al.*, The 2021 magnonics roadmap, J. Phys.: Condens. Matter **33**, 413001 (2021).
[2] A. Mahmoud, F. Ciubotaru, F. Vanderveken, A. V. Chumak, S. Hamdioui, C. Adelmann, and S. Cotofana, Introduction to spin wave computing, J. Appl. Phys. **128**, 161101 (2020).
[3] V. E. Demidov, S. Urazhdin, G. de Loubens, O. Klein, V. Cros, A. Anane, and S. O. Demokritov, Magnetization oscillations and waves driven by pure spin currents, Phys. Rep. **673**, 1 (2017).
[4] D. Grundler, Nanomagnonics around the corner, Nat. Nanotechnol. **11**, 407 (2016).
[5] A. V. Chumak, V. I. Vasyuchka, A. A. Serga, and B. Hillebrands, Magnon spintronics, Nat. Phys. **11**, 453 (2015).
[6] B. Lenk, H. Ulrichs, F. Garbs, and M. Münzenberg, The building blocks of magnonics, Phys. Rep. **507**, 107 (2011).
[7] A. A. Serga, A. V. Chumak, and B. Hillebrands, YIG magnonics, J. Phys. D **43**, 264002 (2010).
[8] J. Chen, H. Wang, T. Hula, C. Liu, S. Liu, T. Liu, H. Jia, Q. Song, C. Guo, Y. Zhang, J. Zhang, X. Han, D. Yu, M. Wu, H. Schultheiss, and H. Yu, Reconfigurable spin-wave interferometer at the nanoscale, Nano Lett. **21**, 6237 (2021).
[9] K. Szulc, P. Graczyk, M. Mruczkiewicz, G. Gubbiotti, and M. Krawczyk, Spin-Wave Diode and Circulator Based on Unidirectional Coupling, Phys. Rev. Appl. **14**, 034063 (2020).
[10] M. Grassi, M. Geilen, D. Louis, M. Mohseni, T. Brächer, M. Hehn, D. Stoeffler, M. Bailleul, P. Pirro, and Y. Henry, Slow-Wave-Based Nanomagnonic Diode, Phys. Rev. Appl. **14**, 024047 (2020).
[11] J. Lan, W. Yu, R. Wu, and J. Xiao, Spin-Wave Diode, Phys. Rev. X **5**, 041049 (2015).
[12] M. Jamali, J. H. Kwon, S.-M. Seo, K.-J. Lee, and H. Yang, Spin wave nonreciprocity for logic device applications, Sci. Rep. **3**, 3160 (2013).
[13] P. Pirro, V. I. Vasyuchka, A. A. Serga, and B. Hillebrands, Advances in coherent magnonics, Nat. Rev. Mater. **6**, 1114 (2021).
[14] V. V. Kruglyak, Chiral magnonic resonators: Rediscovering the basic magnetic chirality in magnonics, Appl. Phys. Lett. **119**, 200502 (2021).
[15] V. V. Kruglyak, S. O. Demokritov, and D. Grundler, Magnonics, J. Phys. D **43**, 264001 (2010).
[16] R. W. Damon and J. R. Eshbach, Magnetostatic modes of a ferromagnet slab, J. Phys. Chem. Solids **19**, 308 (1961).
[17] R. E. Camley, Nonreciprocal surface waves, Surf. Sci. Rep. **7**, 103 (1987).
[18] J. H. Kwon, J. Yoon, P. Deorani, J. M. Lee, J. Sinha, K. J. Lee, M. Hayashi, and H. Yang, Giant nonreciprocal emission of spin waves in Ta/Py bilayers, Sci. Adv. **2**, e1501892 (2016).
[19] T. An, V. I. Vasyuchka, K. Uchida, A. V. Chumak, K. Yamaguchi, K. Harii, J. Ohe, M. B. Jungfleisch, Y. Kajiwara, H. Adachi, B. Hillebrands, S. Maekawa, and E. Saitoh, Unidirectional spin-wave heat conveyer, Nat. Mater. **12**, 549 (2013).
[20] M. Ishibashi, Y. Shiota, T. Li, S. Funada, T. Moriyama, and T. Ono, Switchable giant nonreciprocal frequency shift of propagating spin waves in synthetic antiferromagnets, Sci. Adv. **6**, eaaz6931 (2020).
[21] R. A. Gallardo, T. Schneider, A. K. Chaurasiya, A. Oelschlägel, S. S. P. K. Arekapudi, A. Roldán-Molina, R. Hübner, K. Lenz, A. Barman, J. Fassbender, J. Lindner, O. Hellwig, and P. Landeros, Reconfigurable Spin-Wave Nonreciprocity Induced by Dipolar Interaction in a Coupled Ferromagnetic Bilayer, Phys. Rev. Appl. **12**, 034012 (2019).
[22] K. An, V. S. Bhat, M. Mruczkiewicz, C. Dubs, and D. Grundler, Optimization of Spin-Wave Propagation with Enhanced Group Velocities by Exchange-Coupled Ferrimagnet-Ferromagnet Bilayers, Phys. Rev. Appl. **11**, 034065 (2019).

[23] O. Gladii, M. Haidar, Y. Henry, M. Kostylev, and M. Bailleul, Frequency nonreciprocity of surface spin wave in permalloy thin films, Phys. Rev. B **93**, 054430 (2016).
[24] R. A. Gallardo, P. Alvarado-Seguel, T. Schneider, C. Gonzalez-Fuentes, A. Roldan-Molina, K. Lenz, J. Lindner, and P. Landeros, Spin-wave non-reciprocity in magnetization-graded ferromagnetic films, New J. Phys. **21**, 033026 (2019).
[25] P. Borys, O. Kolokoltsev, N. Qureshi, M. L. Plumer, and T. L. Monchesky, Unidirectional spin wave propagation due to a saturation magnetization gradient, Phys. Rev. B **103**, 144411 (2021).
[26] R. Macêdo, A. S. Kudinoor, K. L. Livesey, and R. E. Camley, Breaking space inversion-symmetry to obtain asymmetric spin-wave excitation in systems with nonuniform magnetic exchange, Adv. Electron. Mater. **8**, 2100435 (2022).
[27] A. V. Sadovnikov, E. N. Beginin, S. E. Sheshukova, Yu. P. Sharaevskii, A. I. Stognij, N. N. Novitski, V. K. Sakharov, Yu. V. Khivintsev, and S. A. Nikitov, Route toward semiconductor magnonics: Light-induced spin-wave nonreciprocity in a YIG/GaAs structure, Phys. Rev. B **99**, 054424 (2019).
[28] S. Tateno and Y. Nozaki, Highly Nonreciprocal Spin Waves Excited by Magnetoelastic Coupling in a Ni/Si Bilayer, Phys. Rev. Appl. **13**, 034074 (2020).
[29] P. J. Shah, D. A. Bas, I. Lisenkov, A. Matyushov, N. X. Sun, and M. R. Page, Giant nonreciprocity of surface acoustic waves enabled by the magnetoelastic interaction, Sci. Adv. **6**, eabc5648 (2020).
[30] X. Zhang, A. Galda, X. Han, D. Jin, and V. M. Vinokur, Broadband Nonreciprocity Enabled by Strong Coupling of Magnons and Microwave Photons, Phys. Rev. Appl. **13**, 044039 (2020).
[31] Y.-P. Wang, J. W. Rao, Y. Yang, P.-C. Xu, Y. S. Gui, B. M. Yao, J. Q. You, and C.-M. Hu, Nonreciprocity and Unidirectional Invisibility in Cavity Magnonics, Phys. Rev. Lett. **123**, 127202 (2019).
[32] Q. Wang, M. Kewenig, M. Schneider, R. Verba, F. Kohl, B. Heinz, M. Geilen, M. Mohseni, B. Lägel, F. Ciubotaru, C. Adelmann, C. Dubs, S. D. Cotofana, O. V. Dobrovolskiy, T. Brächer, P. Pirro, and A. V. Chumak, A magnonic directional coupler for integrated magnonic half-adders, Nat. Electron. **3**, 765 (2020).
[33] A. V. Chumak, A. A. Serga, and B. Hillebrands, Magnon transistor for all-magnon data processing, Nat. Commun. **5**, 4700 (2014).
[34] M. Mohseni, R. Verba, T. Brächer, Q. Wang, D. A. Bozhko, B. Hillebrands, and P. Pirro, Backscattering Immunity of Dipole-Exchange Magnetostatic Surface Spin Waves, Phys. Rev. Lett. **122**, 197201 (2019).
[35] K. L. Wong, L. Bi, M. Bao, Q. Wen, J. P. Chatelon, Y.-T. Lin, C. A. Ross, H. Zhang, and K. L. Wang, Unidirectional propagation of magnetostatic surface spin waves at a magnetic film surface, Appl. Phys. Lett. **105**, 232403 (2014).
[36] X. S. Wang, H. W. Zhang, and X. R. Wang, Topological Magnonics: A Paradigm for Spin-Wave Manipulation and Device Design, Phys. Rev. Appl. **9**, 024029 (2018).
[37] X. S. Wang, Y. Su, and X. R. Wang, Topologically protected unidirectional edge spin waves and beam splitter, Phys. Rev. B **95**, 014435 (2017).
[38] Z.-X. Li, Y. Cao, and P. Yan, Topological insulators and semimetals in classical magnetic systems, Phys. Rep. **915**, 1 (2021).
[39] Z.-X. Li, C. Wang, Y. Cao, and P. Yan, Edge states in a two-dimensional honeycomb lattice of massive magnetic skyrmions, Phys. Rev. B **98**, 180407(R) (2018).
[40] A. Mook, J. Henk, and I. Mertig, Edge states in topological magnon insulators, Phys. Rev. B **90**, 024412 (2014).
[41] R. Shindou, J. Ohe, R. Matsumoto, S. Murakami, and E. Saitoh, Chiral spin-wave edge modes in dipolar magnetic thin films, Phys. Rev. B **87**, 174402 (2013).
[42] L. Udvardi and L. Szunyogh, Chiral Asymmetry of the Spin-Wave Spectra in Ultrathin Magnetic Films, Phys. Rev. Lett. **102**, 207204 (2009).
[43] H. Wang, J. L. Chen, T. Liu, J. Y. Zhang, K. Baumgaertl, C. Y. Guo, Y. H. Li, C. P. Liu, P. Che, S. Tu, S. Liu, P. Gao, X. F. Han, D. Yu, M. Z. Wu, D. Grundler, and H. Yu, Chiral Spin-Wave Velocities Induced by All-Garnet Interfacial Dzyaloshinskii-Moriya Interaction in Ultrathin Yttrium Iron Garnet Films, Phys. Rev. Lett. **124**, 027203 (2020).
[44] H. Bouloussa, Y. Roussigné, M. Belmeguenai, A. Stashkevich, S.-M. Chérif, S. D. Pollard, and H. Yang, Dzyaloshinskii-Moriya interaction induced asymmetry in dispersion of magnonic Bloch modes, Phys. Rev. B **102**, 014412 (2020).
[45] A. Hrabec, Z. Luo, L. J. Heyderman, and P. Gambardella, Synthetic chiral magnets promoted by the Dzyaloshinskii-Moriya interaction, Appl. Phys. Lett. **117**, 130503 (2020).
[46] R. A. Gallardo, D. Cortés-Ortuño, T. Schneider, A. Roldán-Molina, F. Ma, R. E. Troncoso, K. Lenz, H. Fangohr, J. Lindner, and P. Landeros, Flat Bands, Indirect Gaps, and Unconventional Spin-Wave Behavior Induced by a Periodic Dzyaloshinskii-Moriya Interaction, Phys. Rev. Lett. **122**, 067204 (2019).
[47] Y. Sun, H. Chang, M. Kabatek, Y.-Y. Song, Z. Wang, M. Jantz, W. Schneider, M. Wu, E. Montoya, B. Kardasz, B. Heinrich, S. G. E. te Velthuis, H. Schultheiss, and A. Hoffmann, Damping in Yttrium Iron Garnet Nanoscale Films Capped by Platinum, Phys. Rev. Lett. **111**, 106601 (2013).
[48] Y. Au, E. Ahmad, O. Dmytriiev, M. Dvornik, T. Davison, and V. V. Kruglyak, Resonant microwave-to-spin-wave transducer, Appl. Phys. Lett. **100**, 182404 (2012).
[49] Y. Au, M. Dvornik, O. Dmytriiev, and V. V. Kruglyak, Nanoscale spin wave valve and phase shifter, Appl. Phys. Lett. **100**, 172408 (2012).
[50] J. L. Chen, T. Yu, C. P. Liu, T. Liu, M. Madami, K. Shen, J. Y. Zhang, S. Tu, M. S. Alam, K. Xia, M. Z. Wu, G. Gubbiotti, Y. M. Blanter, G. E. W. Bauer, and H. Yu, Excitation of unidirectional exchange spin waves by a nanoscale magnetic grating, Phys. Rev. B **100**, 104427 (2019).
[51] H. Wang, J. Chen, T. Yu, C. Liu, C. Guo, S. Liu, K. Shen, H. Jia, T. Liu, J. Zhang, and M. A. Cabero, Nonreciprocal coherent coupling of nanomagnets by exchange spin waves, Nano Res. **14**, 2133 (2021).
[52] J. Chen, J. Hu, and H. Yu, Chiral emission of exchange spin waves by magnetic skyrmions, ACS Nano **15**, 4372 (2021).
[53] K. G. Fripp, A. V. Shytov, and V. V. Kruglyak, Spin-wave control using dark modes in chiral magnonic resonators, Phys. Rev. B **104**, 054437 (2021).
[54] M. Sushruth, M. Grassi, K. Ait-Oukaci, D. Stoeffler, Y. Henry, D. Lacour, M. Hehn, U. Bhaskar, M. Bailleul, T. Devolder, and J.-P. Adam, Electrical spectroscopy of forward volume spin waves in perpendicularly magnetized materials, Phys. Rev. Res. **2**, 043203 (2020).

[55] V. F. Dmitriev and B. A. Kalinikos, Excitation of propagating magnetization waves by microstrip antennas, Sov. Phys. J. **31**, 875 (1988).
[56] T. Schneider, A. A. Serga, T. Neumann, B. Hillebrands, and M. P. Kostylev, Phase reciprocity of spin-wave excitation by a microstrip antenna, Phys. Rev. B **77**, 214411 (2008).
[57] V. E. Demidov, M. P. Kostylev, K. Rott, P. Krzysteczko, G. Reiss, and S. O. Demokritov, Excitation of microwaveguide modes by a stripe antenna, Appl. Phys. Lett. **95**, 112509 (2009).
[58] K. Kasahara, M. Nakayama, X. Ya, K. Matsuyama, and T. Manago, Effect of distance between a magnet layer and an excitation antenna on the nonreciprocity of magnetostatic surface waves, Jpn. J. Appl. Phys. **56**, 010309 (2017).
[59] H. Yu, O. D. Kelly, V. Cros, R. Bernard, P. Bortolotti, A. Anane, F. Brandl, F. Heimbach, and D. Grundler, Approaching soft x-ray wavelengths in nanomagnet-based microwave technology, Nat. Commun. **7**, 11255 (2016).
[60] C. Liu, J. Chen, T. Liu, F. Heimbach, H. Yu, Y. Xiao, J. Hu, M. Liu, H. Chang, T. Stueckler, S. Tu, Y. Zhang, Y. Zhang, P. Gao, Z. Liao, D. Yu, K. Xia, N. Lei, W. Zhao, and M. Wu, Long-distance propagation of short-wavelength spin waves, Nat. Commun. **9**, 738 (2018).
[61] P. Che, K. Baumgaertl, A. Kúkol'ová, C. Dubs, and D. Grundler, Efficient wavelength conversion of exchange magnons below 100 nm by magnetic coplanar waveguides, Nat. Commun. **11**, 1445 (2020).
[62] T. Yu, C. Liu, H. Yu, Y. M. Blanter, and G. E. W. Bauer, Chiral excitation of spin waves in ferromagnetic films by magnetic nanowire gratings, Phys. Rev. B **99**, 134424 (2019).
[63] T. Yu, Y. M. Blanter, and G. E. W. Bauer, Chiral Pumping of Spin Waves, Phys. Rev. Lett. **123**, 247202 (2019).
[64] D. D. Stancil and A. Prabhakar, *Spin Waves: Theory and Applications* (Springer, New York, 2009).
[65] A. Vansteenkiste, J. Leliaert, M. Dvornik, M. Helsen, F. Garcia-Sanchez, and B. Van Waeyenberge, The design and verification of MUMAX3, AIP Adv. **4**, 107133 (2014).
[66] Z. Zhang, H. Yang, Z. Wang, Y. Cao, and P. Yan, Strong coupling of quantized spin waves in ferromagnetic bilayers, Phys. Rev. B **103**, 104420 (2021).
[67] S. O. Demokritov, B. Hillebrands, and A. N. Slavin, Brillouin light scattering studies of confined spin waves: Linear and nonlinear confinement, Phys. Rep. **348**, 441 (2001).
[68] B. A. Kalinikos and A. N. Slavin, Theory of dipole-exchange spin wave spectrum for ferromagnetic films with mixed exchange boundary conditions, J. Phys. C **19**, 7013 (1986).
[69] D. Kumar, O. Dmytriiev, S. Ponraj, and A. Barman, Numerical calculation of spin wave dispersions in magnetic nanostructures, J. Phys. D **45**, 015001 (2012).
[70] T. Yu and G. E. W. Bauer, Chiral coupling to magnetodipolar radiation, Top. Appl. Phys. **138**, 1 (2021).
[71] S. Yawale and S. Yawale, Differential amplifier, in *Operational Amplifier: Theory and Experiments* (Springer, Singapore, 2022), pp. 1–25.
[72] S. V. Vasiliev, V. V. Kruglyak, M. L. Sokolovskii, and A. N. Kuchko, Spin wave interferometer employing a local nonuniformity of the effective magnetic field, J. Appl. Phys. **101**, 113919 (2007).
[73] M. P. Kostylev, A. A. Serga, T. Schneider, T. Neumann, B. Leven, B. Hillebrands, and R. L. Stamps, Resonant and nonresonant scattering of dipole-dominated spin waves from a region of inhomogeneous magnetic field in a ferromagnetic film, Phys. Rev. B **76**, 184419 (2007).
[74] S. O. Demokritov, A. A. Serga, A. André, V. E. Demidov, M. P. Kostylev, B. Hillebrands, and A. N. Slavin, Tunneling of Dipolar Spin Waves through a Region of Inhomogeneous Magnetic Field, Phys. Rev. Lett. **93**, 047201 (2004).
[75] M. Xu, K. Yamamoto, J. Puebla, K. Baumgaertl, B. Rana, K. Miura, H. Takahashi, D. Grundler, S. Maekawa, and Y. Otani, Nonreciprocal surface acoustic wave propagation via magneto-rotation coupling, Sci. Adv. **6**, eabb1724 (2020).
[76] Y. Henry, O. Gladii, and M. Bailleul, Propagating spin-wave normal modes: A dynamic matrix approach using plane-wave demagnetizing tensors, arXiv:1611.06153.
[77] V. E. Demidov, S. Urazhdin, H. Ulrichs, V. Tiberkevich, A. Slavin, D. Baither, G. Schmitz, and S. O. Demokritov, Magnetic nano-oscillator driven by pure spin current, Nat. Mater. **11**, 1028 (2012).
[78] C. Safranski, I. Barsukov, H. K. Lee, T. Schneider, A. A. Jara, A. Smith, H. Chang, K. Lenz, J. Lindner, Y. Tserkovnyak, M. Wu, and I. N. Krivorotov, Spin caloritronic nano-oscillator, Nat. Commun. **8**, 117 (2017).
[79] Z. Zhang, M. Vogel, J. Holanda, M. B. Jungfleisch, C. Liu, Y. Li, J. E. Pearson, R. Divan, W. Zhang, A. Hoffmann, Y. Nie, and V. Novosad, Spin-wave frequency division multiplexing in an yttrium iron garnet microstripe magnetized by inhomogeneous field, Appl. Phys. Lett. **115**, 232402 (2019).
[80] J. D. Jackson, *Classical Electrodynamics* (Wiley, New York, 1962).
[81] M. Bailleul, Spectroscopie d'ondes de spin pour l'électronique de spin, habilitation thesis, University of Strasbourg, 2011.
[82] R. Verba, V. Tiberkevich, and A. Slavin, Spin-wave transmission through an internal boundary: Beyond the scalar approximation, Phys. Rev. B **101**, 144430 (2020).